

3D thermo-hydro-mechanical coupled discrete beam lattice model of saturated poro-plastic medium

Emina Hadzalic^{*1,3}, Adnan Ibrahimbegovic^{1,2a} and Samir Dolarevic^{3b}

¹Université de Technologie de Compiègne, Laboratoire Roberval de Mécanique,
Centre de Recherche Royallieu, 60200 Compiègne, France

²Institut Universitaire de France, France

³Faculty of Civil Engineering, University of Sarajevo, Patriotske lige 30, Sarajevo 71000,
Bosnia and Herzegovina

(Received January 17, 2020, Revised March 3, 2020, Accepted March 25, 2020)

Abstract. In this paper, we present a 3D thermo-hydro-mechanical coupled discrete beam lattice model of structure built of the nonisothermal saturated poro-plastic medium subjected to mechanical loads and nonstationary heat transfer conditions. The proposed model is based on Voronoi cell representation of the domain with cohesive links represented as inelastic Timoshenko beam finite elements enhanced with additional kinematics in terms of embedded strong discontinuities in axial and both transverse directions. The enhanced Timoshenko beam finite element is capable of modeling crack formation in mode I, mode II and mode III. Mode I relates to crack opening, mode II relates to in-plane crack sliding, and mode III relates to the out-of-plane shear sliding. The pore fluid flow and heat flow in the proposed model are governed by Darcy's law and Fourier's law for heat conduction, respectively. The pore pressure field and temperature field are approximated with linear tetrahedral finite elements. By exploiting nodal point quadrature rule for numerical integration on tetrahedral finite elements and duality property between Voronoi diagram and Delaunay tetrahedralization, the numerical implementation of the coupling results with additional pore pressure and temperature degrees of freedom placed at each node of a Timoshenko beam finite element. The results of several numerical simulations are presented and discussed.

Keywords: coupled discrete beam lattice model; saturated porous medium; pore pressure; temperature; coupling; localized failure; temperature dependent parameters

1. Introduction

The pioneering works in the domain of isothermal solid phase-pore fluid interaction are Terzaghi's theory of one-dimensional consolidation (Terzaghi 1944), and Biot's theory of three-dimensional consolidation (Biot 1941), with both theories being limited to the case of elastic porous media. The isothermal solid phase-pore fluid interaction is further extended to the nonisothermal case in order to account for the temperature effects in the saturated porous media. The pioneering work in the finite element analysis of thermo-hydro-mechanical coupling problem is the work of

*Corresponding author, Ph.D., E-mail: emina.hadzalic@utc.fr, emina.hadzalic@gf.unsa.ba

^aProfessor, E-mail: adnan.ibrahimbegovic@utc.fr

^bProfessor, E-mail: samir.dolarevic@gf.unsa.ba

Aboustit *et al.* (Aboustit 1983, Aboustit *et al.* 1985), followed by the works of (Britto *et al.* 1992, Lewis *et al.* 1986, Lewis *et al.* 1989, Noorishad and Tsang 1996, Gatmiri and Delage 1997, Cui *et al.* 2018).

Taking these developments a one step further in order to be able to predict the overall safety of structure built of saturated porous media, a numerical model of the structure has to be able to capture cracking and localized failure in the structure subjected to extreme loads. Here, the extreme loads include not only the mechanical loads but the thermal loads as well (Ostermann and Dinkler 2014, Ngo *et al.* 2014). Namely, temperature changes can induce additional stresses in the structure as a result of restrained movement, which may contribute to cracking. Furthermore, the thermal actions can affect the stiffness and strength properties of the material, which has to be properly accounted for in order to provide a sound design of the structure. To be able to model these phenomena, which influence the overall safety and durability of the structure, the numerical model of the pore-saturated structure has to account for the thermal coupling.

In this paper, we propose a thermo-hydro-mechanical coupled discrete beam lattice model of structure built of the nonisothermal saturated poro-plastic medium. The latter is the main novelty of the proposed model with respect to 2D plain strain coupled discrete beam lattice model presented in (Nikolic *et al.* 2015, Nikolic *et al.* 2016, Hadzalic *et al.* 2018a, b, c, Hadzalic *et al.* 2019). The plain strain coupled discrete beam lattice model is extended to the 3D case, and the thermal coupling is added to the model in order to account for the temperature effects in saturated poro-plastic media. The proposed 3D model is based on Voronoi cell representation of the domain with cohesive links as inelastic Timoshenko beam finite elements enhanced with additional kinematics in terms of embedded strong discontinuities in axial and both transverse directions. The pore fluid flow and heat flow in the model are defined with Darcy's law and Fourier's law for heat conduction, respectively. The pore pressure field and the temperature field are discretized with linear tetrahedral finite elements, resulting with additional pore pressure and temperature degrees of freedom placed at each node of the Timoshenko beam finite element.

The outline of the paper is as follows: In Section 2, we describe the equations governing the response of the nonisothermal saturated porous medium. In Section 3, we present the finite element formulation of the proposed thermo-hydro-mechanical coupled discrete beam lattice model, together with the computational procedure. In Section 4, we present the results of several numerical simulations with the aim to validate the proposed coupled discrete beam lattice model of structure built of a nonisothermal saturated porous medium, and to demonstrate its capabilities to predict response and cracking in the structure subjected to combined thermal and mechanical loads. In Section 5, we give some concluding remarks.

2. Governing equations of nonisothermal saturated porous medium

The equations governing the response of nonisothermal saturated porous medium are derived by combining equilibrium equation imposed on a porous medium, continuity equation imposed on a fluid flow and energy equation imposed on heat flow through such a porous medium (Aboustit 1983, Aboustit *et al.* 1985, Lewis *et al.* 1986, Lewis and Schrefler 1998). The governing equations are derived under the assumption that no phase change occurs and that the thermal equilibrium between the solid phase and the pore fluid is achieved.

2.1 Equilibrium equation

The strong form of equilibrium equation is written as

$$\nabla \cdot \boldsymbol{\sigma} + \mathbf{b} = \mathbf{0} \quad (1)$$

where $\boldsymbol{\sigma}$ is the nominal stress tensor, and \mathbf{b} is the body forces vector.

Following Terzaghi's principle of effective stresses, the nominal stress is decomposed into effective stress and pore pressure, written as

$$\boldsymbol{\sigma} = \boldsymbol{\sigma}' - \mathbf{I}bp \quad (2)$$

where $\boldsymbol{\sigma}'$ is the effective stress tensor, \mathbf{I} is the second order identity tensor, p is the pore pressure (assumed positive if compression), and b is Biot's constant.

Furthermore, the effective stress tensor can be decomposed into mechanical part $\boldsymbol{\sigma}_u$ resulting from nonhomogeneous displacements and thermal part $\boldsymbol{\sigma}_T$, resulting from corresponding changes in temperature, written as

$$\boldsymbol{\sigma}' = \boldsymbol{\sigma}_u - \boldsymbol{\sigma}_T \quad (3)$$

with $\boldsymbol{\sigma}_T$ computed as

$$\boldsymbol{\sigma}_T = \boldsymbol{\beta}_T (T - T_0) \quad (4)$$

where T_0 is the reference temperature, and $\boldsymbol{\beta}_T$ is the thermal stress tensor for isotropic case defined as

$$\boldsymbol{\beta}_T = \beta_T \mathbf{I} \quad (5)$$

2.2 Continuity equation

The continuity equation governing the fluid flow through a nonisothermal porous medium (for the usual temperature dependence of the solid density neglected) can be written as

$$\frac{1}{M} \dot{p} + b \nabla \cdot \dot{\mathbf{u}} - \bar{\beta}_{sf} \dot{T} - \nabla \cdot \left(\frac{k}{\gamma_f} \nabla p \right) = 0 \quad (6)$$

where M is Biot's modulus, k is the coefficient of permeability of the isotropic porous medium, γ_f is the specific weight of the fluid and $\bar{\beta}_{sf}$ is the thermal expansion coefficient of the mixture defined as

$$\bar{\beta}_{sf} = (b - n) \bar{\beta}_s + n \bar{\beta}_f \quad (7)$$

with n as the porosity, $\bar{\beta}_s$ as the thermal expansion coefficient of the solid phase and $\bar{\beta}_f$ as the thermal expansion coefficient of the pore fluid.

2.3 Energy equation

The energy equation for porous medium under the assumption that both the solid phase and pore fluid have the same temperature at the coincident point and with convection ignored is written as

$$\rho C_T \dot{T} + \nabla \cdot \mathbf{q}_T - s = 0 \quad (8)$$

where \mathbf{q}_T is the heat flux, s is the heat source, and ρC_T is the effective heat capacity defined as

$$\rho C_T = (1-n)\rho_s C_T^s + n\rho_f C_T^f \quad (9)$$

with ρ_s , C_T^s as the mass density and heat capacity of the solid phase and ρ_f , C_T^f as the mass density and heat capacity of the pore fluid.

The heat flux \mathbf{q}_T is defined with the Fourier's law for heat conduction, written as

$$\nabla \cdot \mathbf{q}_T = -k_T \nabla T \quad (10)$$

where k_T is the coefficient of thermal conductivity of the isotropic porous medium.

In the formulation of the energy equation, the convection, the pressure and temperature dependence of the solid and fluid densities, and mechanical contributions to energy balance are neglected. These simplifications are, in many cases, justified and result in an uncoupled form of the energy equation (Lewis *et al.* 1986, Lewis and Schrefler 1998, Booker and Savvidou 1985).

3. Coupled discrete beam lattice model of nonisothermal pore-saturated structure

The starting point for our work on coupled discrete beam lattice model of the nonisothermal pore-saturated structure is the 2D plain strain coupled discrete beam lattice model presented in (Nikolic *et al.* 2015, Nikolic *et al.* 2016, Hadzalic *et. al* 2018a, b, c, Hadzalic *et. al* 2019) for the isothermal case.

For the numerical representation of the structure built of a nonisothermal saturated poro-plastic medium, we extend the proposed 2D plane strain coupled discrete beam lattice model to the 3D setting, and we introduce the thermal coupling into the model. For the construction of the discrete lattice model in the 3D framework, we exploit the duality property between the Voronoi cell representation and Delaunay tetrahedralization of the domain (Fig. 1). The end result of Delaunay

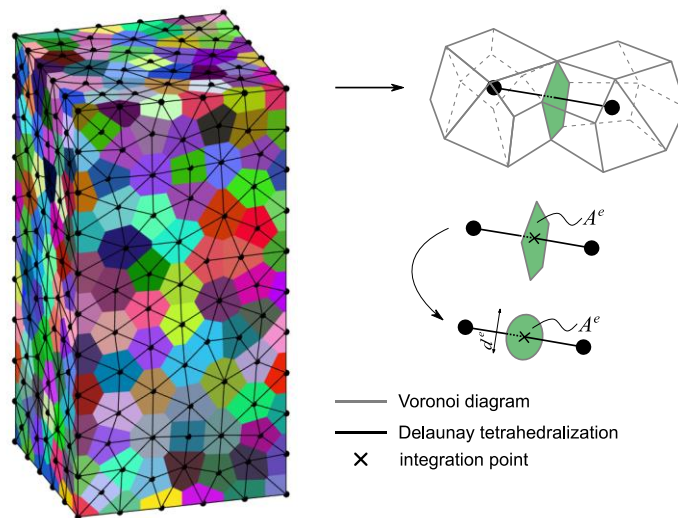


Fig. 1 Voronoi diagram and Delaunay tetrahedralization

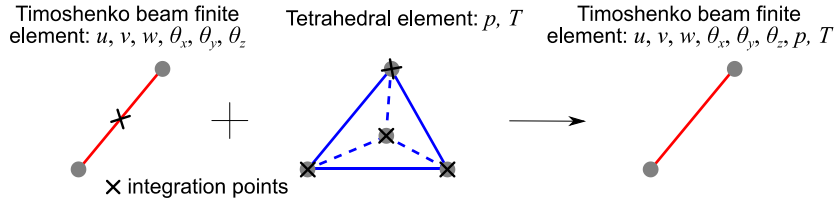


Fig. 2 Displacement, pore pressure and temperature fields finite element approximations

tetrahedralization is the mesh of tetrahedra. Every edge of tetrahedra connects the centers of two adjacent Voronoi cells and is perpendicular to the polygon shared between these two cells. We place along each edge of tetrahedra a cohesive link, whose behavior we model with the beam finite element. The cross-section of each beam finite element is the polygon shared between two adjacent cells. In general case, the polygonal cross-section for every beam finite element is of a different shape. To simplify these computations, we replace the polygonal cross-section for every finite element with an equivalent circular cross-section (Fig. 1). More precisely, we compute the diameter of an equivalent circular cross-section from the condition that the area of the polygon obtained from Voronoi cell representation is equal to the area of a circular cross-section.

The fracture behavior of cohesive links is modeled with inelastic Timoshenko beam finite elements enhanced with additional kinematics in terms of embedded discontinuities in axial and both transverse directions (Nikolic and Ibrahimbegovic 2015). Thus, enhanced Timoshenko beam finite element is capable of modeling crack formation in mode I, mode II and mode III. Mode I relates to crack opening, mode II relates to in-plane crack sliding, and mode III relates to the out-of-plane shear sliding. It is important to note that linear elastic parameters of Timoshenko beam finite element, Young's modulus E and Poisson's ratio ν can be identified from the condition that no stiffness is gained or lost compared to the 3D continuum (Hadzalic *et al.* 2019). However, other parameters such as yield and fracture limits have to be identified through more elaborate parameter identification procedures such as those probability based ones (e.g., Karavelić *et al.* 2019).

In a 3D numerical model of structure built of a nonisothermal saturated poro-plastic medium, we spread the pore fluid flow and heat flow across the mesh of tetrahedra (Tet4 - linear tetrahedral finite elements) that coincides with the mesh of tetrahedra obtained by Delaunay tetrahedralization of the domain. For numerical integration on tetrahedral finite elements, we choose nodal point rule, which positions the integration points at every node of tetrahedral (Gellert and Harbord 1991). The integration rule of this kind eliminates the contribution of two nodes that do not belong to the beam and only includes the contribution of the two nodes that belong to the Timoshenko beam finite element. This allows us to treat the pore pressure and the temperature as additional degrees of freedom placed at each node of the Timoshenko beam finite element (Fig. 2).

Next, we present the finite element formulation of the 3D coupled discrete beam lattice model for nonisothermal pore-saturated structures.

3.1 Finite element formulation

3.1.1 Kinematics

Consider a straight Timoshenko beam finite element of length L^e and cross-sectional area A^e . All equations for Timoshenko beam finite element are expressed in a local coordinate frame, which can be easily adapted to the global frame by using standard local-global transformation (Fig. 3).

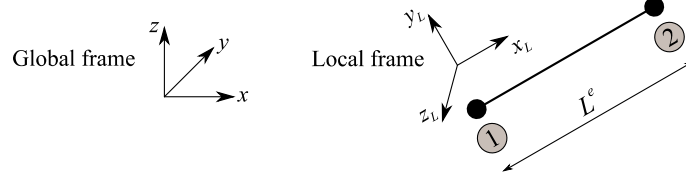


Fig. 3 Local and global coordinate frame

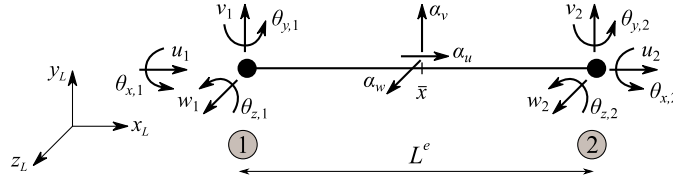


Fig. 4 Timoshenko beam finite element in 3D framework

The element has two nodes, and six degrees of freedom per node: axial displacement u along local x axis, transverse displacements v and w along local y and z axes, and rotations of cross-section $\theta_x, \theta_y, \theta_z$ around local x, y, z axes, respectively (Fig. 4). For simplicity, we considered a Timoshenko beam placed along the global x axis. The displacement fields are enhanced in axial and both transverse directions with embedded strong discontinuities in order to model the corresponding three modes of crack formation. The enhanced displacement fields are interpolated as

$$\mathbf{u} = \mathbf{N}_u^s \bar{\mathbf{u}} + \mathbf{M} \boldsymbol{\alpha} \quad (11)$$

where

$$\begin{aligned} \mathbf{u}^T &= \{u, v, w, \theta_x, \theta_y, \theta_z\} \\ \bar{\mathbf{u}}^T &= \{u_1, v_1, w_1, \theta_{x,1}, \theta_{y,1}, \theta_{z,1}, u_2, v_2, w_2, \theta_{x,2}, \theta_{y,2}, \theta_{z,2}\} \\ \boldsymbol{\alpha}^T &= \{\alpha^u, \alpha^v, \alpha^w, 0, 0, 0\} \\ \mathbf{N}_u^s &= \begin{bmatrix} N_1 & 0 & 0 & 0 & 0 & 0 & N_2 & 0 & 0 & 0 & 0 & 0 \\ 0 & N_1 & 0 & 0 & 0 & 0 & 0 & N_2 & 0 & 0 & 0 & 0 \\ 0 & 0 & N_1 & 0 & 0 & 0 & 0 & 0 & N_2 & 0 & 0 & 0 \\ 0 & 0 & 0 & N_1 & 0 & 0 & 0 & 0 & 0 & N_2 & 0 & 0 \\ 0 & 0 & 0 & 0 & N_1 & 0 & 0 & 0 & 0 & 0 & N_2 & 0 \\ 0 & 0 & 0 & 0 & 0 & N_1 & 0 & 0 & 0 & 0 & 0 & N_2 \end{bmatrix}; \quad \{N_1, N_2\} = \left\{1 - \frac{x}{L^e}, \frac{x}{L^e}\right\} \\ \mathbf{M} &= \begin{bmatrix} M & 0 & 0 & 0 & 0 & 0 \\ 0 & M & 0 & 0 & 0 & 0 \\ 0 & 0 & M & 0 & 0 & 0 \\ 0 & 0 & 0 & 0 & 0 & 0 \\ 0 & 0 & 0 & 0 & 0 & 0 \\ 0 & 0 & 0 & 0 & 0 & 0 \end{bmatrix}; \quad M = H_{\bar{x}} - N_2; \quad H_{\bar{x}} = \begin{cases} 0, & x \leq \bar{x} \\ 1, & x > \bar{x} \end{cases} \end{aligned} \quad (12)$$

Here, α_u, α_v and α_w represent displacement jumps in axial direction, in-plane transverse and out-of-plane transverse directions.

The enhanced strain fields are interpolated as

$$\mathbf{u} = \mathbf{N}_u^s \bar{\mathbf{u}} + \mathbf{M} \boldsymbol{\alpha} \quad (11)$$

where

$$\boldsymbol{\varepsilon}^T = \{\varepsilon, \gamma_y, \gamma_z, \kappa_x, \kappa_y, \kappa_z\} \Rightarrow \begin{cases} \varepsilon = \frac{du}{dx} & \kappa_x = \frac{d\theta_x}{dx} \\ \gamma_y = \frac{dv}{dx} - \theta_z & \kappa_y = \frac{d\theta_y}{dx} \\ \gamma_z = \frac{dw}{dx} + \theta_y & \kappa_z = \frac{d\theta_z}{dx} \end{cases} \quad (14)$$

$$\mathbf{B}_u^s = \begin{bmatrix} B_1 & 0 & 0 & 0 & 0 & 0 & B_2 & 0 & 0 & 0 & 0 & 0 \\ 0 & B_1 & 0 & 0 & 0 & -N_1 & 0 & B_2 & 0 & 0 & 0 & -N_2 \\ 0 & 0 & B_1 & 0 & N_1 & 0 & 0 & 0 & B_2 & 0 & N_2 & 0 \\ 0 & 0 & 0 & B_1 & 0 & 0 & 0 & 0 & 0 & B_2 & 0 & 0 \\ 0 & 0 & 0 & 0 & B_1 & 0 & 0 & 0 & 0 & 0 & B_2 & 0 \\ 0 & 0 & 0 & 0 & 0 & B_1 & 0 & 0 & 0 & 0 & 0 & B_2 \end{bmatrix}; \quad \mathbf{G} = \begin{bmatrix} G & 0 & 0 & 0 & 0 & 0 \\ 0 & G & 0 & 0 & 0 & 0 \\ 0 & 0 & G & 0 & 0 & 0 \\ 0 & 0 & 0 & 0 & 0 & 0 \\ 0 & 0 & 0 & 0 & 0 & 0 \\ 0 & 0 & 0 & 0 & 0 & 0 \end{bmatrix}; \quad (15)$$

$$\{B_1, B_2\} = \left\{ \frac{dN_1}{dx}, \frac{dN_2}{dx} \right\} = \left\{ -\frac{1}{L}, \frac{1}{L} \right\}; \quad G = \frac{dM}{dx} = \begin{cases} \bar{G}, & x \in [0, \bar{x}) \cup (\bar{x}, L^e] \\ \bar{G} + \delta_{\bar{x}}, & x = \bar{x} \\ \delta_{\bar{x}} = \begin{cases} 0, & x \in [0, \bar{x}) \cup (\bar{x}, L^e] \\ \infty, & x = \bar{x} \end{cases} \end{cases}$$

where ε is the axial strain, γ_y, γ_z are the shear strains, and $\kappa_x, \kappa_y, \kappa_z$ are the curvatures.

The pore pressure field and temperature fields are approximated with tetrahedral finite elements with four nodes (Fig. 5). The finite element approximations for the pore pressure field and temperature field can be written as

$$p = \mathbf{N}_p^s \bar{\mathbf{p}}; \quad T = \mathbf{N}_T^s \bar{\mathbf{T}} \quad (16)$$

$$\bar{\mathbf{p}}^T = \{p_1, p_2, p_3, p_4\}; \quad \bar{\mathbf{T}}^T = \{T_1, T_2, T_3, T_4\}$$

$$\mathbf{N}_p^s = \{N_1^p, N_2^p, N_3^p, N_4^p\}; \quad \mathbf{N}_T^s = \{N_1^T, N_2^T, N_3^T, N_4^T\}; \quad N_i^p = N_i^T = \frac{a_i + b_i x + c_i y + d_i z}{6V}; \quad i = 1, 4;$$

$$6V = \det \begin{bmatrix} 1 & x_1 & y_1 & z_1 \\ 1 & x_2 & y_2 & z_2 \\ 1 & x_3 & y_3 & z_3 \\ 1 & x_4 & y_4 & z_4 \end{bmatrix}; \quad a_1 = \det \begin{bmatrix} x_2 & y_2 & z_2 \\ x_3 & y_3 & z_3 \\ x_4 & y_4 & z_4 \end{bmatrix}; \quad b_1 = -\det \begin{bmatrix} 1 & y_2 & z_2 \\ 1 & y_3 & z_3 \\ 1 & y_4 & z_4 \end{bmatrix}; \quad (17)$$

$$c_1 = -\det \begin{bmatrix} x_2 & 1 & z_2 \\ x_3 & 1 & z_3 \\ x_4 & 1 & z_4 \end{bmatrix}; \quad d_1 = \det \begin{bmatrix} x_2 & y_2 & 1 \\ x_3 & y_3 & 1 \\ x_4 & y_4 & 1 \end{bmatrix};$$

etc.

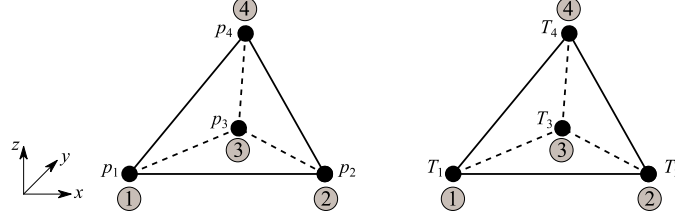


Fig. 5 Pore pressure and temperature fields finite element approximations

where V is the volume of the tetrahedral element, x, y, z are global coordinates, x_i, y_i, z_i are nodal coordinates of tetrahedral element, and constants $a_{2,4}, b_{2,4}, c_{2,4}, d_{2,4}$ are defined by the cyclic interchange of the subscripts in the order 1,2,3,4.

The time derivative of displacement, pore pressure and temperature fields are written as

$$\dot{\mathbf{u}} = \mathbf{N}_u^s \dot{\bar{\mathbf{u}}}; \quad \dot{p} = \mathbf{N}_p^s \dot{\bar{p}}; \quad \dot{T} = \mathbf{N}_T^s \dot{\bar{T}} \quad (18)$$

3.1.2 Weak form of governing equations

Continuity equation: The coupling of the mechanics and the pore fluid flow occurs through the axial direction of the Timoshenko beam finite element. The continuity equation is written as

$$\frac{1}{M} \dot{p} + b\dot{\epsilon} - \bar{\beta}_{sf} \dot{T} - \nabla \cdot \left(\frac{k}{\gamma_f} \nabla p \right) = 0 \quad (19)$$

By introducing the finite element discrete approximations into the weak form of continuity equation, we obtain

$$\int_{\Omega_{tet4}^e} \left[\left(\mathbf{N}_p^{s,T} \frac{1}{M} \mathbf{N}_p^s \right) \dot{\bar{p}} - \left(\mathbf{N}_p^{s,T} \bar{\beta}_{sf} \mathbf{N}_p^s \right) \dot{\bar{T}} + \left((\nabla \mathbf{N}_p^s)^T \frac{k}{\gamma_f} \nabla \mathbf{N}_p^s \right) \bar{p} \right] d\Omega + \int_0^L \left(\mathbf{N}_{up}^{s,T} b \mathbf{B}_{up}^s \right) \dot{\bar{\mathbf{u}}} dx = \mathbf{q}^{ext,e} \quad (20)$$

where

$$\mathbf{N}_{up}^s = \{N_1, N_2\}; \quad \mathbf{B}_{up}^s = [B_1 \ 0 \ 0 \ 0 \ 0 \ 0 \ B_2 \ 0 \ 0 \ 0 \ 0 \ 0] \quad (21)$$

Energy equation: The energy equation is written as

$$\rho C_T \dot{T} + \nabla \cdot (k_T \nabla T) - s = 0 \quad (22)$$

By performing the standard finite element discretization procedure, we obtain

$$\int_{\Omega_{tet4}^e} \left[\left(\mathbf{N}_T^{s,T} \rho C_T \mathbf{N}_T^s \right) \dot{\bar{T}} + \left((\nabla \mathbf{N}_T^s)^T k_T \nabla \mathbf{N}_T^s \right) \bar{T} \right] d\Omega = \mathbf{s}^{ext,e} \quad (23)$$

Equilibrium equation: The weak form of equilibrium equations for the Timoshenko beam finite element is derived from the principle of virtual works. By exploiting the principle of virtual works and performing standard finite element discretization procedure, we obtain the corresponding equations where the first equation relates to the equilibrium in the bulk part of the element, and the

second equation relates to the equilibrium at the discontinuity, written as

$$\begin{aligned} \mathbf{f}^{int,e} - \mathbf{f}^{ext,e} &= \mathbf{0} \\ \mathbf{h}^e &= \mathbf{0} \end{aligned} \tag{24}$$

where

$$\begin{aligned} \mathbf{f}^{int,e} &= \int_0^{L^e} \mathbf{B}_u^{s,T} \boldsymbol{\sigma} dx = \mathbf{f}^{int,e}(\boldsymbol{\sigma}_{uT}) - \mathbf{f}^{int,e}(\boldsymbol{\sigma}_p) \\ \mathbf{h}^e &= \int_0^{L^e} \mathbf{G}^T \boldsymbol{\sigma}_{uT} dx = \int_0^{L^e} \bar{\mathbf{G}}^T \boldsymbol{\sigma}_{uT} dx + \mathbf{t}; \quad \bar{\mathbf{G}} = \begin{bmatrix} \bar{G} & 0 & 0 & 0 & 0 & 0 \\ 0 & \bar{G} & 0 & 0 & 0 & 0 \\ 0 & 0 & \bar{G} & 0 & 0 & 0 \\ 0 & 0 & 0 & 0 & 0 & 0 \\ 0 & 0 & 0 & 0 & 0 & 0 \\ 0 & 0 & 0 & 0 & 0 & 0 \end{bmatrix} \\ & \mathbf{t}^T = \{t^u, t^v, t^w, 0, 0, 0\} \\ \boldsymbol{\sigma}^T &= \{N, V_y, V_z, M_x, M_y, M_z\}; \\ \boldsymbol{\sigma}^T &= \boldsymbol{\sigma}_{uT} - \boldsymbol{\sigma}_p; \\ \boldsymbol{\sigma}_{uT}^T &= \{N'_{uT}, V'_{uT,y}, V'_{uT,z}, M'_{uT,x}, M'_{uT,y}, M'_{uT,z}\}; \quad \boldsymbol{\sigma}_p^T = \{bp^e A^e, 0, 0, 0, 0, 0\}; \\ & p^e = \mathbf{N}_{up}^s \bar{\mathbf{p}}; \quad \bar{\mathbf{p}}^T = \{p_1, p_2\}; \\ \boldsymbol{\sigma}_{uT}^T &= \boldsymbol{\sigma}_u^T - \boldsymbol{\sigma}_T^T; \\ \boldsymbol{\sigma}_u^T &= \{N', V'_y, V'_z, M'_x, M'_y, M'_z\}; \quad \boldsymbol{\sigma}_T^T = \{\beta_T^{uT} (T - T_0) A^e, 0, 0, 0, 0, 0\}; \\ & T = \mathbf{N}_{uT}^s \bar{\mathbf{T}}; \quad \bar{\mathbf{T}}^T = \{T_1, T_2\}; \end{aligned} \tag{25}$$

Here, $N = N' - bp^e A^e$ is the total axial force, whereas $V_y = V'_y$ and $V_z = V'_z$ are the shear forces, and finally $M_x = M'_x$ is the torsion moment, while $M_y = M'_y$ and $M_z = M'_z$ are the bending moments (Fig. 6). The superscript ' denotes effective force. Here, we assume that the coupling of the mechanics and the internal fluid flow occurs through the axial direction of the Timoshenko beam finite element. Next, \mathbf{t} is the internal force vector acting at the discontinuity and β_T^{uT} is the thermal stress for thermo-mechanical coupling in the axial direction.

The stress resultants $N', V'_y, V'_z, M'_x, M'_y, M'_z$ are computed from the selected constitutive model for the Timoshenko beam finite element. For axial and both transverse directions, the pre-

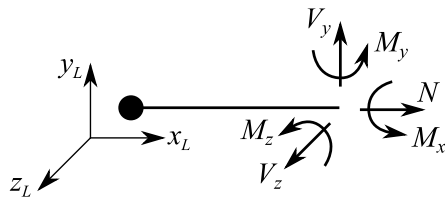


Fig. 6 Stress resultants

peak response of the element is described with the elasto-viscoplastic constitutive model with both linear isotropic hardening (Ibrahimbegovic 2009), and Fredrick-Armstrong nonlinear kinematic hardening law (Armstrong and Frederick 1966). The post-peak response of the element is described with exponential softening. More details on the selected constitutive model can be found in (Nikolic *et al.* 2015, Nikolic and Ibrahimbegovic 2015, Nikolic *et al.* 2016, Hadzalic *et al.* 2018 a, b, c, Ismar *et al.* 2015, Hadzalic *et al.* 2019). The behavior of the element in bending and torsion remains purely linear elastic.

For linear elasticity, the thermal stress β_T^{ut} is a function of lattice Young's modulus E and thermal expansion coefficient of the solid phase $\bar{\beta}_s$, which can be written as

$$\beta_T^{ut} = Ek_{\beta_T^{ut}} \bar{\beta}_s \quad (26)$$

The coefficient $k_{\beta_T^{ut}}$ takes into account the difference between 1D thermo-mechanical coupling and the 3D thermo-mechanical coupling. Namely, in 3D thermo-mechanical coupling for isotropic case the thermal stress β_T can be expressed in terms of thermal expansion coefficient $\bar{\beta}_s$ and Lamé's parameters for the continuum model λ_L and μ_L , written as

$$\beta_T = (3\lambda_L + 2\mu_L) \bar{\beta}_s \quad (27)$$

The last expression can be rewritten in terms of oedometer modulus E_{oed} and Poisson's ratio ν for the continuum model, as

$$\beta_T = \left(\frac{1+\nu}{1-\nu} \right) E_{oed} \bar{\beta}_s \quad (28)$$

Hence, the coefficient $k_{\beta_T^{ut}}$ can then be computed as

$$k_{\beta_T^{ut}} = \left(\frac{1+\nu}{1-\nu} \right) E_{oed} / E \quad (29)$$

3.1.4 Computational procedure

The system of equations governing the thermo-hydro-mechanical coupled problem for single Timoshenko beam finite element is written as

$$\begin{aligned} \mathbf{f}^{int,e}(\boldsymbol{\sigma}_{uT}) - \mathbf{K}_{up}^e \bar{\mathbf{p}} &= \mathbf{f}^{ext,e} \\ \mathbf{K}_{up}^{e,T} \dot{\bar{\mathbf{u}}} - \mathbf{K}_{pT}^e \dot{\bar{\mathbf{T}}} + \mathbf{D}_{pp}^e \dot{\bar{\mathbf{p}}} + \mathbf{K}_{pp}^e \bar{\mathbf{p}} &= \mathbf{q}^{ext,e} \\ \mathbf{D}_{TT}^e \dot{\bar{\mathbf{T}}} + \mathbf{K}_{TT}^e \bar{\mathbf{T}} &= \mathbf{s}^{ext,e} \end{aligned} \quad (30)$$

where $\mathbf{f}^{int,e}(\boldsymbol{\sigma}_{uT})$ is the internal load vector resulting from displacements and temperature changes, \mathbf{K}_{up}^e and \mathbf{K}_{pT}^e are the coupling matrices, \mathbf{D}_{pp}^e is the compressibility matrix, \mathbf{K}_{pp}^e is the permeability matrix, \mathbf{D}_{TT}^e is the heat capacity matrix, \mathbf{K}_{TT}^e is the conductivity matrix, and $\mathbf{f}^{ext,e}$, $\mathbf{q}^{ext,e}$, $\mathbf{s}^{ext,e}$, are the load vectors. The matrices \mathbf{K}_{up}^e , \mathbf{K}_{pT}^e , \mathbf{D}_{pp}^e , \mathbf{K}_{pp}^e , \mathbf{D}_{TT}^e and \mathbf{K}_{TT}^e are computed as

$$\begin{aligned}
 \mathbf{K}_{up}^e &= \int_0^{L^e} \mathbf{B}_{up}^{s,T} b \mathbf{N}_{up}^s dx; & \mathbf{K}_{pT}^e &= \int_{\Omega_{Ter4}^e} \mathbf{N}_p^{s,T} \bar{\beta}_{sf} \mathbf{N}_T^s d\Omega \\
 \mathbf{D}_{pp}^e &= \int_{\Omega_{Ter4}^e} \mathbf{N}_p^{s,T} \frac{1}{M} \mathbf{N}_p^s d\Omega; & \mathbf{K}_{pp}^e &= \int_{\Omega_{Ter4}^e} (\nabla \mathbf{N}_p^s)^T \frac{k}{\gamma_f} \nabla \mathbf{N}_p^s d\Omega \\
 \mathbf{D}_{TT}^e &= \int_{\Omega_{Ter4}^e} \mathbf{N}_T^{s,T} \rho C_T \mathbf{N}_T^s d\Omega; & \mathbf{K}_{TT}^e &= \int_{\Omega_{Ter4}^e} (\nabla \mathbf{N}_T^s)^T k_T \nabla \mathbf{N}_T^s d\Omega
 \end{aligned} \tag{31}$$

Here we note that in the global system of equations (Eq. (30)) we take the parts of the \mathbf{D}_{pp}^e , \mathbf{K}_{pp}^e , \mathbf{K}_{pT}^e , \mathbf{D}_{TT}^e and \mathbf{K}_{TT}^e matrices (Eq. (31)) that correspond to the nodes of Timoshenko beam finite element.

The solution in terms of unknown nodal displacements, pore pressures and temperatures is computed at discrete pseudo-time steps t_1, t_2, \dots, t_n using backward Euler time-integration scheme. For a time step t_{n+1} and iteration i , the global system of equations to be solved is written as

$$\sum_{e=1}^{n_{elem}} \mathbf{A} \left\{ \begin{bmatrix} \bar{\mathbf{K}}_{uu} & -\mathbf{K}_{up} & -\bar{\mathbf{K}}_{uT} \\ \frac{1}{\Delta t} \mathbf{K}_{up}^T & \frac{1}{\Delta t} \mathbf{D}_{pp} + \mathbf{K}_{pp} & \frac{1}{\Delta t} \mathbf{K}_{pT} \\ 0 & 0 & \frac{1}{\Delta t} \mathbf{D}_{TT} + \mathbf{K}_{TT} \end{bmatrix}_{n+1} \right\}^{e,(i)} = \left\{ \begin{matrix} \left\{ \Delta \bar{\mathbf{u}} \right\}_{n+1}^{e,(i)} \\ \left\{ \Delta \bar{\mathbf{p}} \right\}_{n+1} \\ \left\{ \Delta \bar{\mathbf{T}} \right\}_{n+1} \end{matrix} \right\} = \left\{ \begin{matrix} \left\{ \mathbf{r}_u \right\}_{n+1}^{e,(i)} \\ \left\{ \mathbf{r}_p \right\}_{n+1} \\ \left\{ \mathbf{r}_T \right\}_{n+1} \end{matrix} \right\} \tag{32}$$

where $\bar{\mathbf{K}}_{uu}^e$ is the tangent stiffness matrix, $\bar{\mathbf{K}}_{uT}^e$ is the tangent coupling matrix, and $\mathbf{r}_u^e, \mathbf{r}_p^e, \mathbf{r}_T^e$ are residuals pertaining to the solid, the pore fluid and the temperature part.

After solving the global system of equations, the new iterative values of unknown fields are updated as

$$\begin{aligned}
 \bar{\mathbf{u}}_{n+1}^{(i+1)} &= \bar{\mathbf{u}}_{n+1}^{(i)} + \Delta \bar{\mathbf{u}}_{n+1}^{(i)} \\
 \bar{\mathbf{p}}_{n+1}^{(i+1)} &= \bar{\mathbf{p}}_{n+1}^{(i)} + \Delta \bar{\mathbf{p}}_{n+1}^{(i)} \\
 \bar{\mathbf{T}}_{n+1}^{(i+1)} &= \bar{\mathbf{T}}_{n+1}^{(i)} + \Delta \bar{\mathbf{T}}_{n+1}^{(i)}
 \end{aligned} \tag{33}$$

The correct tangent stiffness matrix $\bar{\mathbf{K}}_{uu}^e$ and tangent coupling matrix $\bar{\mathbf{K}}_{uT}^e$ is chosen depending if the element is in elasto-viscoplastic or softening part of the response.

If the element is elasto-viscoplastic, the tangent stiffness matrix and tangent coupling matrix are defined as

$$\begin{aligned}
 \bar{\mathbf{K}}_{uu,n+1}^{e,(i)} &= \mathbf{K}_{uu,n+1}^{e,(i)} = \left(\frac{\partial \mathbf{f}^{int}(\boldsymbol{\sigma}_{uT})}{\partial \bar{\mathbf{u}}} \right)_{n+1}^{e,(i)} = \int_0^{L^e} \mathbf{B}_u^{s,T} \mathbf{C}_{n+1}^{ep,u,(i)} \mathbf{B}_u^s dx \\
 \bar{\mathbf{K}}_{uT,n+1}^{e,(i)} &= \mathbf{K}_{uT,n+1}^{e,(i)} = \left(\frac{\partial \mathbf{f}^{int}(\boldsymbol{\sigma}_{uT})}{\partial \bar{\mathbf{T}}} \right)_{n+1}^{e,(i)} = \int_0^{L^e} \mathbf{B}_{uT}^{s,T} C_{n+1}^{ep,u,(i)} k_{\beta_{sf}} \bar{\beta}_s A^e \mathbf{N}_{uT}^s dx \\
 \mathbf{B}_{uT}^s &= [B_1 \quad 0 \quad 0 \quad 0 \quad 0 \quad 0 \quad B_2 \quad 0 \quad 0 \quad 0 \quad 0 \quad 0]
 \end{aligned} \tag{34}$$

where elasto-plastic tangent matrix is written as

$$\mathbf{C}_{n+1}^{ep,(i)} = \begin{bmatrix} \mathbf{C}_{n+1}^{ep,u} A^e & 0 & 0 & 0 & 0 & 0 \\ 0 & \mathbf{C}_{n+1}^{ep,v} A^e & 0 & 0 & 0 & 0 \\ 0 & 0 & \mathbf{C}_{n+1}^{ep,w} A^e & 0 & 0 & 0 \\ 0 & 0 & 0 & GI_{pol}^e & 0 & 0 \\ 0 & 0 & 0 & 0 & EI^e & 0 \\ 0 & 0 & 0 & 0 & 0 & EI^e \end{bmatrix} \quad (35)$$

where $\mathbf{C}_{n+1}^{ep,u}$, $\mathbf{C}_{n+1}^{ep,v}$, $\mathbf{C}_{n+1}^{ep,w}$ are elasto-plastic tangent moduli for axial and transverse directions, G is the shear modulus, and I^e, I_{pol}^e are the second moment of inertia and polar moment of inertia for a circular cross section, respectively.

If the element is in the softening regime, the tangent stiffness matrix and tangent coupling matrix are obtained by performing a static condensation procedure in which the unknown values of displacement jumps are eliminated from the condition that the residual at the discontinuity is equal to zero. The statically condensed tangent stiffness matrix is written as

$$\bar{\mathbf{K}}_{uu,n+1}^{e,(i)} = \hat{\mathbf{K}}_{uu,n+1}^{e,(i)} = \left[\mathbf{K}_{uu,n+1}^{e,(i)} - \mathbf{F}_{n+1}^{e,(i)} \left(\mathbf{H}_{n+1}^{e,(i)} + \mathbf{K}_\alpha \right)^{-1} \left(\mathbf{F}_{n+1}^{e,(i),T} + \mathbf{K}_d \right) \right] \quad (36)$$

where

$$\begin{aligned} \bar{\mathbf{K}}_{uu,n+1}^{e,(i)} &= \left(\frac{\partial \mathbf{f}^{int}(\boldsymbol{\sigma}_{uT})}{\partial \bar{\mathbf{u}}} \right)_{n+1}^{e,(i)} = \int_0^{L^e} \mathbf{B}_u^{s,T} \mathbf{C}_{n+1}^{ep,(i)} \mathbf{B}_u^s dx \\ \mathbf{F}_{n+1}^{e,(i)} &= \left(\frac{\partial \mathbf{f}^{int}(\boldsymbol{\sigma}_{uT})}{\partial \boldsymbol{\alpha}} \right)_{n+1}^{e,(i)} = \int_0^{L^e} \mathbf{B}_u^{s,T} \mathbf{C}_{n+1}^{ep,(i)} \bar{\mathbf{G}} dx \\ \left(\mathbf{F}^T + \mathbf{K}_d \right)_{n+1}^{e,(i)} &= \left(\frac{\partial \mathbf{h}}{\partial \bar{\mathbf{u}}} \right)_{n+1}^{e,(i)} = \int_0^{L^e} \bar{\mathbf{G}}^T \mathbf{C}_{n+1}^{ep,(i)} \mathbf{B}_u^s dx + \mathbf{K}_d \\ \left(\mathbf{H} + \mathbf{K}_\alpha \right)_{n+1}^{e,(i)} &= \left(\frac{\partial \mathbf{h}}{\partial \boldsymbol{\alpha}} \right)_{n+1}^{e,(i)} = \int_0^{L^e} \bar{\mathbf{G}}^T \mathbf{C}_{n+1}^{ep,(i)} \bar{\mathbf{G}} dx + \mathbf{K}_\alpha \end{aligned} \quad (37)$$

The matrices \mathbf{K}_d and \mathbf{K}_α depend on the current step in softening being elastic or plastic. If the current step in the softening is elastic, then

$$\mathbf{K}_d = \mathbf{C}^* \mathbf{B}_u^s; \quad \mathbf{K}_\alpha = \mathbf{0}; \quad \mathbf{C}^* = \begin{bmatrix} EA^e & 0 & 0 & 0 & 0 & 0 \\ 0 & k_c GA^e & 0 & 0 & 0 & 0 \\ 0 & 0 & k_c GA^e & 0 & 0 & 0 \\ 0 & 0 & 0 & 0 & 0 & 0 \\ 0 & 0 & 0 & 0 & 0 & 0 \\ 0 & 0 & 0 & 0 & 0 & 0 \end{bmatrix} \quad (38)$$

where k_c is the shear correction factor.

Else, if the current step in the softening is plastic, then we get

$$\mathbf{K}_d = \mathbf{0}; \quad \mathbf{K}_\alpha = \begin{bmatrix} K_\alpha^u A^e & 0 & 0 & 0 & 0 & 0 \\ 0 & K_\alpha^v A^e & 0 & 0 & 0 & 0 \\ 0 & 0 & K_\alpha^w A^e & 0 & 0 & 0 \\ 0 & 0 & 0 & 0 & 0 & 0 \\ 0 & 0 & 0 & 0 & 0 & 0 \\ 0 & 0 & 0 & 0 & 0 & 0 \end{bmatrix} \quad (39)$$

where $K_\alpha^u, K_\alpha^v, K_\alpha^w$ for exponential softening take the following form

$$K_\alpha^j = -\frac{(\sigma_f^j)^2}{G_f^j} \left(\exp\left(-\bar{\xi}^j \frac{\sigma_f^j}{G_f^j}\right) \right); \quad j = u, v, w \quad (40)$$

Here, σ_f is the fracture limit, G_f is the fracture energy and $\bar{\xi}$ is the strain-like softening variable.

By taking into account that the coupling of solid phase with fluid flow occurs through the axial direction of the Timoshenko beam finite element, the statically condensed tangent coupling matrix is written as

$$\bar{\mathbf{K}}_{uT, n+1}^{e, (i)} = \hat{\mathbf{K}}_{uT, n+1}^{e, (i)} = \left[\mathbf{K}_{uT, n+1}^{e, (i)} - \mathbf{Q}_{n+1}^{e, (i)} \left(\mathbf{Y}_{n+1}^{e, (i)} + \mathbf{K}_{\alpha T} \right)^{-1} \left(\mathbf{W}_{n+1}^{e, (i), T} + \mathbf{K}_T \right) \right] \quad (41)$$

where

$$\begin{aligned} \bar{\mathbf{K}}_{uu, n+1}^{e, (i)} &= \left(\frac{\partial \mathbf{f}^{int}(\boldsymbol{\sigma}_{uT})}{\partial \bar{\mathbf{T}}} \right)_{n+1}^{e, (i)} = \int_0^{L^e} \mathbf{B}_{uT}^{s, T} C_{n+1}^{ep, u, (i)} k_{\beta uT} \bar{\beta}_s A^e \mathbf{N}_{uT}^s dx \\ \mathbf{Q}_{n+1}^{e, (i)} &= \left(\frac{\partial \mathbf{f}^{int}(\boldsymbol{\sigma}_{uT})}{\partial \boldsymbol{\alpha}} \right)_{n+1}^{e, (i)} = \int_0^{L^e} \mathbf{B}_{uT}^{s, T} C_{n+1}^{ep, u, (i)} k_{\beta uT} \bar{\beta}_s A^e \bar{G} dx \\ (\mathbf{W}^T + \mathbf{K}_T)_{n+1}^{e, (i)} &= \left(\frac{\partial \mathbf{h}}{\partial \bar{\mathbf{T}}} \right)_{n+1}^{e, (i)} = \int_0^{L^e} \bar{G}^T C_{n+1}^{ep, (i)} k_{\beta uT} \bar{\beta}_s A^e \mathbf{N}_{uT}^s dx + \mathbf{K}_T \\ (\mathbf{Y} + \mathbf{K}_{\alpha T})_{n+1}^{e, (i)} &= \left(\frac{\partial \mathbf{h}}{\partial \boldsymbol{\alpha}} \right)_{n+1}^{e, (i)} = \int_0^{L^e} \bar{G}^T C_{n+1}^{ep, (i)} A^e \bar{G} dx + \mathbf{K}_{\alpha T} \end{aligned} \quad (42)$$

The matrices \mathbf{K}_T and $\mathbf{K}_{\alpha T}$ depend on the current step in softening being elastic or plastic. If the current step in the softening is elastic, then

$$\mathbf{K}_T = C_{n+1}^{ep, u, (i)} A^e \mathbf{N}_{uT}^s; \quad \mathbf{K}_{\alpha T} = 0 \quad (43)$$

Else, if the current step in the softening is plastic, then

$$\mathbf{K}_T = 0; \quad \mathbf{K}_{\alpha T} = K_\alpha^u A^e \quad (44)$$

4. Numerical results

In this section, we present the results of several numerical simulations, which serve to illustrate the proposed approach ability to deal with nonisothermal problems. All numerical implementations and computations are performed with the research version of the computer code FEAP, developed by Taylor (Zienkiewicz and Taylor 2005). In all numerical simulations, the finite element mesh is generated by using Delaunay tetrahedralization and GMSH software (Geuzaine and Remacle 2009). The cross-sectional properties of the Timoshenko beam finite elements are computed from Voronoi diagram by using MATLAB software, which uses Qhull code (Barber *et al.* 1996).

4.1 Nonisothermal saturated poro-elastic column

In this section, we perform a thermo-elastic one-dimensional consolidation analysis of saturated

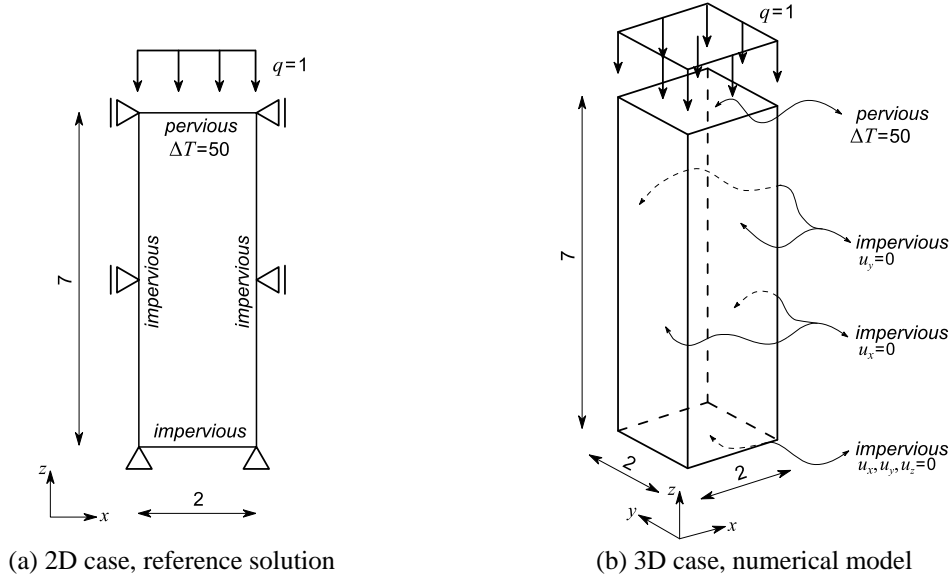


Fig. 7 Thermo-elastic consolidation of saturated column, problem statement

column, with the aim to validate the coupled discrete beam lattice model of structure built of the saturated nonisothermal porous medium. The problem of one-dimensional thermo-elastic consolidation was first solved by Aboustit *et al.* (Aboustit 1983, Aboustit *et al.* 1985), and is later used as a benchmark by Lewis *et al.* (Lewis *et al.* 1986), Noorishad and Tsang (Noorishad and Tsang 1996), Cui *et al.* (Cui *et al.* 2018) to test their finite element formulations in 2D framework. To test our model, we extend the problem analyzed in the literature for 2D case (Fig. 7(a)) to the 3D case (Fig. 7(b)) and we compare our results against reference solutions provided by Lewis *et al.* (Lewis *et al.* 1986) and Cui *et al.* (Cui *et al.* 2018). Since the consolidation analyzed here is the problem of one-dimensional consolidation, the results computed for the 3D case should match those obtained for the 2D case. The problem analyzed here is unit-less.

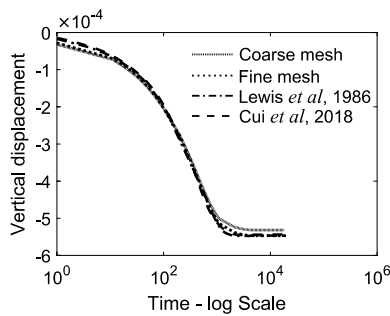
With the aim of inspecting the possible mesh dependency of the results, we perform a computation with a discrete model for two different mesh densities: coarse with 1437 Timoshenko beam finite elements, and fine with 2875 Timoshenko beam finite elements.

The linear elastic parameters of the continuum model are: Young's modulus $E=6000$, and Poisson's ratio $\nu=0.4$, which results with a value of oedometer modulus $E_{oed}=12857$. The identified linear elastic parameters of the Timoshenko beam finite element are: Young's modulus $E=16463$ and Poisson's ratio $\nu=0$. The coefficient of permeability is $k/\gamma_f=4 \cdot 10^{-6}$, Biot's constant is $b=1$ and Biot's modulus is $1/M \rightarrow 0$. The coefficient of thermal conductivity is $k_T=0.2$, the effective heat capacity is $\rho C_T=40$, the thermal expansion coefficient of the solid phase is $\bar{\beta}_s=0.3 \cdot 10^{-6}$ and the reference temperature is $T_0=0$, for both continuum and discrete model. The temperature term in the continuity equation is omitted, i.e., $\bar{\beta}_{sf}$ is set to 0. The coefficient k_{pT} is identified as 1.82.

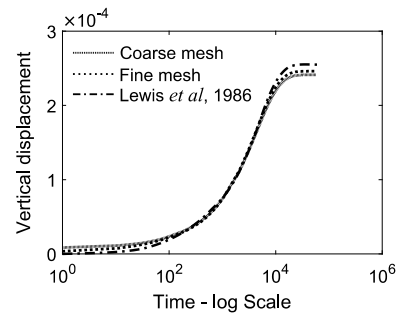
The saturated poro-elastic column (Fig. 7(b)) is subjected to unit vertical surface pressure and constant surface temperature $T=50$. The time step values used in the numerical simulations are indicated in Table 1 (Lewis *et al.* 1986, Cui *et al.* 2018).

Table 1 Time stepping scheme

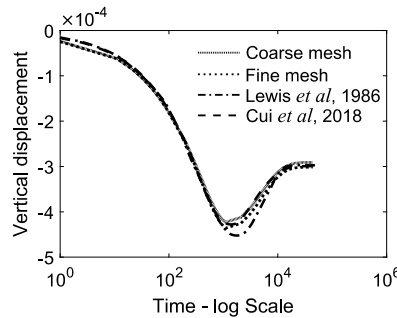
Time interval	Number of time steps
0.01	10
0.1	10
10	10
100	10
1000	20



(a) Isothermal case



(b) Thermal case: surface temperature



(c) Thermal case: surface temperature and pressure

Fig. 8 Saturated poro-elastic column: vertical displacement of column top

We perform three types of computations. The first is the isothermal consolidation with the applied surface pressure only, the second is the thermal consolidation with the applied surface temperature only, and the third is the thermal consolidation with applied both the surface temperature and the surface pressure.

The computed results in terms of vertical displacements of the column top for all three cases are shown in Figs. 8(a)-(c). We can conclude that there exists a good match between the computed results and reference values. The computed results are practically mesh independent. We note that the results for the thermal consolidation with the applied surface temperature only are not given for comparison in (Cui *et al.* 2018)

The computed excess pore pressure and temperature at the $z=6.0$ m measured from the bottom of the column for the third - thermal consolidation case are shown in Figs. 9(a)-(b). We observe a good match between the computed results and reference solutions, with results being practically mesh independent.

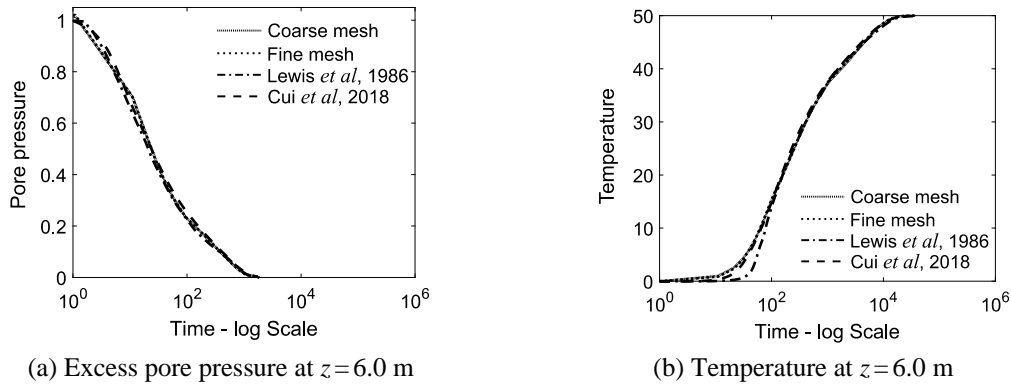


Fig. 9 Thermal case, applied surface temperature and pressure: computed results

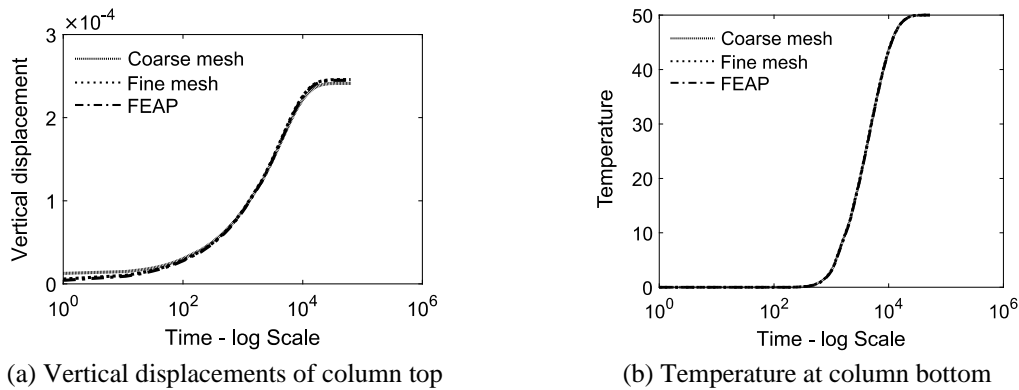


Fig. 10 Thermo-mechanical computation, applied surface temperature: comparison with 3D numerical model in FEAP

Next, we perform a thermo-mechanical computation (the pore pressure field is excluded from the computation) for the case of applied surface temperature only, and we compare the computed results with those obtained with the 3D numerical model of a column constructed by using FEAP built-in solid elements (Zienkiewicz and Taylor 2005). We can conclude that a very good match between computed results is obtained (Figs. 10(a)-(b)). The temperature evolution computed with the discrete model is shown in Figs. 11(a)-(c).

The results presented in this section, suggest that the coefficient of thermal conductivity, the effective heat capacity and thermal expansion coefficient of the coupled discrete beam lattice model closely match those of an equivalent continuum model. Hence, they can be easily identified from standard experimental tests.

4.2 Combined thermal and mechanical compression test

In this section, we perform a combined thermal and mechanical compression test. We first subject the specimen to high temperatures, after which we impose vertical displacements on the top base of the specimen. The geometry of the specimen and the boundary conditions are shown in Fig. 12(a). The finite element mesh is shown in Fig. 12(b).

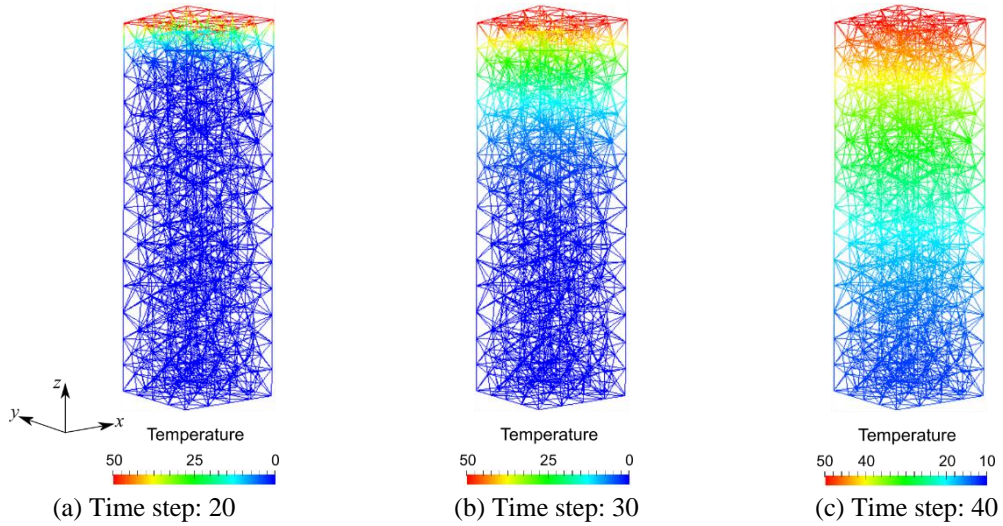


Fig. 11 Temperature evolution, applied surface temperature

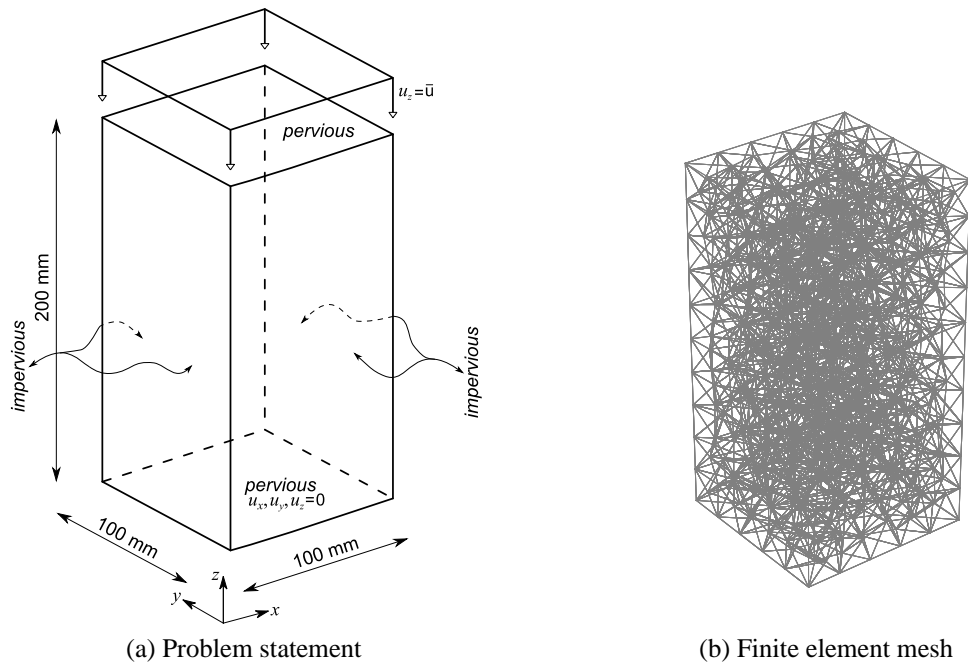


Fig. 12 Thermal mechanical compression test

Table 2 Mechanical properties of the Timoshenko beam finite element

Young's modulus [kPa]	Poisson's ratio [/]	Yield limit [kPa]	Fracture limit [kPa]	Fracture energy [kN/m]
$E=20000$	$\nu=0.2$	$\sigma_{y,t}=10$	$\sigma_{f,t}=12$	$G_{f,t}=20$
		$\sigma_{y,c}=100$	$\sigma_{f,c}=100$	$G_{f,c}=100$
		$\sigma_{y,s}=12$	$\sigma_{f,s}=15$	$G_{f,s}=100$

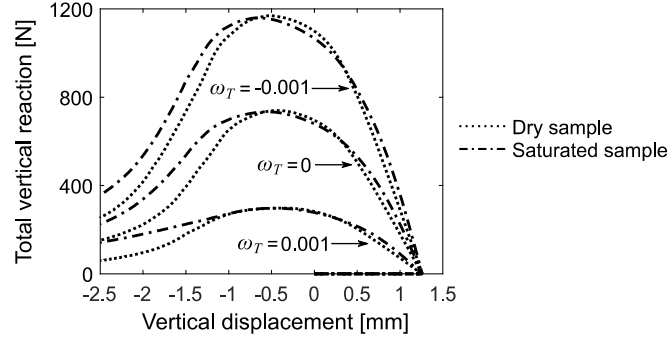


Fig. 13 Thermal mechanical compression test: computed results

The material parameters of the Timoshenko beam finite element are shown in Table 2. The linear hardening modulus is $H_{lh}=2 \cdot 10^3$ kPa, the linear kinematic hardening modulus is $H_{lk}=2 \cdot 10^3$ kPa, nonlinear hardening parameter is $H_{nlk}=2 \cdot 10^2$, and the viscosity parameter is $\eta=20$ kPa s. The coefficient of permeability is $k=10^{-8}$ m/s, the specific weight of the water is $\gamma_w=10$ kN/m³, Biot's constant is $b=1$ and Biot's modulus is $1/M \rightarrow 0$. The coefficient of thermal conductivity is $k_T=2$ W/mK, the effective heat capacity is $\rho C_T=1850$ kJ/Km³, the thermal expansion coefficient of the solid phase is $\bar{\beta}_s=0.0001$ (°C)⁻¹ and the reference temperature is $T_0=0^\circ$. The temperature term in the continuity equation is omitted, i.e., $\bar{\beta}_{sf}$ is set to 0. The coefficient k_{β_T} is selected as 1.0.

To investigate the temperature effects on the stiffness and load carrying capacity of the specimen, we assume that the material parameters: Young's modulus, yield limits, fracture limits and fracture energies of the Timoshenko beam finite element are temperature dependent. We assume linear temperature dependence, written as

$$m = m[1 - \omega_T (T - T_0)]; \quad T > T_0 \quad (45)$$

where m is the material parameter, T and T_0 are the temperature and the reference temperature in the element and ω_T is the parameter controlling the temperature dependence.

Next, we perform several numerical simulations of thermal compression test on dry (Biot's constant $b=0 \rightarrow$ matrix \mathbf{K}_{up} is a null matrix) and saturated specimen (Biot's constant $b=1$) for three values of parameter $\omega_T = -0.001; 0; 0.0001$. We select the same value of ω_T for all material parameters, for which we assumed are temperature dependent. First, we subject the specimen to a temperature of 600°C. After the temperature has reached a steady state throughout the specimen, we impose vertical displacements on the top base of the specimen with a constant rate of $v=1 \cdot 10^{-5}$ m/s.

The computed results are shown in Fig. 13. We can conclude that, depending on the value of ω_T , the stiffness and ultimate load level have decreased or increased when compared to the case of the temperature independent material parameters ($\omega_T=0$). The broken cohesive links in increasing softening at the end of the loading program for saturated specimen and $\omega_T=-0.001$ are shown in Figs. 14(a)-(c).

The value of ω_T depends on the type of material and has to be identified through more elaborate parameter identification procedures. For example, the exposure of the rock or concrete specimen to the elevated temperatures results in a decrease in the compressive strength, whereas for clay specimen the compressive strength increases.

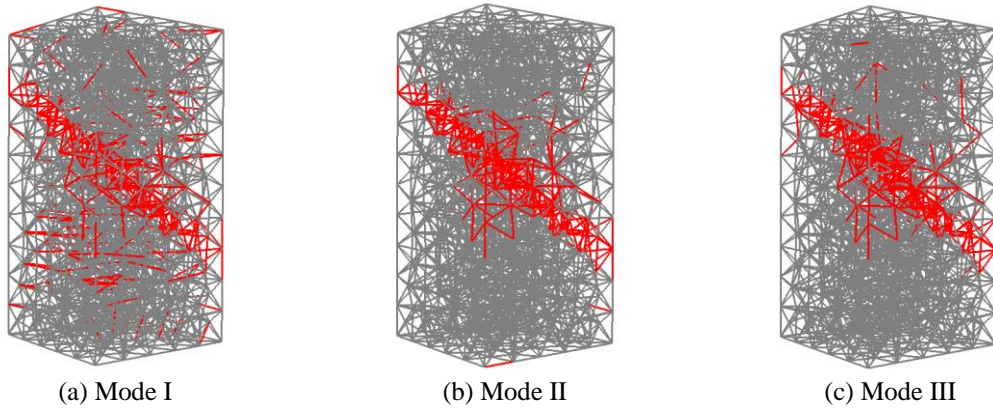


Fig. 14 Failure mode for thermal mechanical compression test, broken cohesive links

5. Conclusions

In this paper, we presented a thermo-hydro-mechanical coupled discrete beam lattice model of structure built of the nonisothermal saturated poro-plastic medium. The mechanical part of the structure response is obtained with a discrete lattice model, which is constructed by exploiting duality property between Voronoi cell representation and Delaunay tetrahedralization of the domain. The behavior of cohesive links is modeled with enhanced Timoshenko beam finite elements. The pore fluid flow and heat flow are introduced in the model through Darcy's law and Fourier's law for heat conduction, respectively. The pore pressure field and the temperature field are approximated with linear tetrahedral finite elements. By exploiting nodal point quadrature rule for numerical integration on tetrahedral finite elements and duality property between Voronoi diagram and Delaunay tetrahedralization, the numerical implementation of the coupling results with additional pore pressure and temperature degrees of freedom placed at each node of a Timoshenko beam finite element.

We have confirmed through the results of validation computations in the linear elastic regime of structure response that the coefficient of thermal conductivity, the effective heat capacity and the thermal expansion coefficient of coupled discrete beam lattice model closely match those of an equivalent continuum model. Hence, they can be easily identified from standard experimental tests.

Finally, we have illustrated the temperature effects on the stiffness and load carrying capacity of the structure by implementing the linear temperature dependence of the material parameters. The parameter controlling the temperature dependence has to be identified through more elaborate parameter identification procedures.

Acknowledgments

This work was supported by the French Ministry of Foreign Affairs, and French Embassy in Bosnia and Herzegovina. Professor Adnan Ibrahimbegovic was supported by the funding for Chaire de Mécanique Picardie (120-2015 RDISTRUCT-000010 and RDISTRUCT-000010) with EU funding (FEDER) and IUF-Institut Universitaire de France (Membre Senior). These grants and financial supports are gratefully acknowledged.

References

- Aboustit, B.L. (1983), "Finite element investigations of thermo-elastic and thermo-plastic consolidation", Ph.D. Dissertation, The Ohio State University, USA.
- Aboustit, B.L., Advani, S.H. and Lee, J.K. (1985), "Variational principles and finite element simulations for thermo-elastic consolidation", *Int. J. Numer. Anal. Meth. Geomech.*, **9**(1), 49-69. <https://doi.org/10.1002/nag.1610090105>.
- Armstrong, P.J. and Frederick, C.O. (1966), "A mathematical representation of the multiaxial Bauschinger effect", CEBG Report RD/B/N, 731.
- Barber, C.B., Dobkin, D.P. and Huhdanpaa, H. (1996), "The quickhull algorithm for convex hulls", *ACM Tran. Math. Softw. (TOMS)*, **22**(4), 469-483. <https://doi.org/10.1145/235815.235821>.
- Biot, M.A. (1941), "General theory of three-dimensional consolidation", *J. Appl. Phys.*, **12**(2), 155-164. <https://doi.org/10.1063/1.1712886>.
- Booker, J.R. and Savvidou, C. (1985), "Consolidation around a point heat source", *Int. J. Numer. Anal. Meth. Geomech.*, **9**(2), 173-184. <https://doi.org/10.1002/nag.1610090206>.
- Britto, A.M., Savvidou, C., Gunn, M.J. and Booker, J.R. (1992), "Finite element analysis of the coupled heat flow and consolidation around hot buried objects", *Soil. Found.*, **32**(1), 13-25. <https://doi.org/10.3208/sandf1972.32.13>.
- Cui, W., Potts, D.M., Zdravković, L., Gawęcka, K.A. and Taborda, D.M.G. (2018), "An alternative coupled thermo-hydro-mechanical finite element formulation for fully saturated soils", *Comput. Geotech.*, **94**, 22-30. <https://doi.org/10.1016/j.compgeo.2017.08.011>.
- Gatmiri, B. and Delage, P. (1997), "A formulation of fully coupled thermal--hydraulic--mechanical behaviour of saturated porous media-numerical approach", *Int. J. Numer. Anal. Meth. Geomech.*, **21**(3), 199-225. [https://doi.org/10.1002/\(SICI\)1096-9853\(199703\)21:3<199::AID-NAG865>3.0.CO;2-M](https://doi.org/10.1002/(SICI)1096-9853(199703)21:3<199::AID-NAG865>3.0.CO;2-M).
- Gellert, M. and Harbord, A. (1991), "Moderate degree cubature formulas for 3-D tetrahedral finite-element approximations", *Commun. Appl. Numer. Meth.*, **7**(6), 487-495. <https://doi.org/10.1002/cnm.1630070609>.
- Geuzaine, C. and Remacle, J.F. (2009), "Gmsh: A 3-D finite element mesh generator with built-in pre- and post-processing facilities", *Int. J. Numer. Meth. Eng.*, **79**(11), 1309-1331. <https://doi.org/10.1002/nme.2579>.
- Hadzalic, E., Ibrahimbegovic, A. and Dolarevic, S. (2018), "Failure mechanisms in coupled soil-foundation systems", *Coupl. Syst. Mech.*, **7**(1), 27-42. <https://doi.org/10.12989/csm.2018.7.1.027>.
- Hadzalic, E., Ibrahimbegovic, A. and Dolarevic, S. (2018), "Fluid-structure interaction system predicting both internal pore pressure and outside hydrodynamic pressure", *Coupl. Syst. Mech.*, **7**(6), 649-668. <https://doi.org/10.12989/csm.2018.7.6.649>.
- Hadzalic, E., Ibrahimbegovic, A. and Dolarevic, S. (2019), "Theoretical formulation and seamless discrete approximation for localized failure of saturated poro-plastic structure interacting with reservoir", *Comput. Struct.*, **214**, 73-93. <https://doi.org/10.1016/j.compstruc.2019.01.003>.
- Hadzalic, E., Ibrahimbegovic, A. and Nikolic, M. (2018), "Failure mechanisms in coupled poro-plastic medium", *Coupl. Syst. Mech.*, **7**(1), 43-59. <https://doi.org/10.12989/csm.2018.7.1.043>.
- Ibrahimbegovic, A. (2009), *Nonlinear Solid Mechanics: Theoretical Formulations and Finite Element Solution Methods*, Springer.
- Imamović, I., Ibrahimbegovic, A. and Knopf-Lenoir, C. (2015), "Plasticity-damage model parameters identification for structural connections", *Coupl. Syst. Mech.*, **4**, 337-364. <http://dx.doi.org/10.12989/csm.2015.4.4.337>.
- Karavelić, E., Nikolić, M., Ibrahimbegovic, A. and Kurtović, A.C. (2019), "Concrete meso-scale model with full set of 3D failure modes with random distribution of aggregate and cement phase. Part I: Formulation and numerical implementation", *Comput. Meth. Appl. Mech. Eng.*, **344**, 1051-1072. <https://doi.org/10.1016/j.cma.2017.09.013>.
- Lewis, R.W. and Schreler, B.A. (1998), *The Finite Element Method in the Static and Dynamic Deformation and Consolidation of Porous Media*, John Wiley.

- Lewis, R.W., Majorana, C.E. and Schrefler, B.A. (1986), "A coupled finite element model for the consolidation of nonisothermal elastoplastic porous media", *Tran. Porous Media*, **1**(2), 155-178. <https://doi.org/10.1007/BF00714690>.
- Lewis, R.W., Roberts, P.J. and Schrefler, B.A. (1989), "Finite element modelling of two-phase heat and fluid flow in deforming porous media", *Tran. Porous Media*, **4**(4), 319-334. <https://doi.org/10.1007/BF00165778>.
- Ngo, V.M., Ibrahimbegovic, A. and Hajdo, E. (2014), "Nonlinear instability problems including localized plastic failure and large deformations for extreme thermo-mechanical conditions", *Coupl. Syst. Mech.*, **3**(1), 89-110. <https://doi.org/10.12989/csm.2014.3.1.089>.
- Nikolic, M. and Ibrahimbegovic, A. (2015), "Rock mechanics model capable of representing initial heterogeneities and full set of 3D failure mechanisms", *Comput. Meth. Appl. Mech. Eng.*, **290**, 209-227. <https://doi.org/10.1016/j.cma.2015.02.024>.
- Nikolic, M., Ibrahimbegovic, A. and Miscevic, P. (2015), "Brittle and ductile failure of rocks: Embedded discontinuity approach for representing mode I and mode II failure mechanisms", *Int. J. Numer. Meth. Engng.*, **102**(8), 1507-1526. <https://doi.org/10.1002/nme.4866>.
- Nikolic, M., Ibrahimbegovic, A. and Miscevic, P. (2016), "Discrete element model for the analysis of fluid-saturated fractured poro-plastic medium based on sharp crack representation with embedded strong discontinuities", *Comput. Meth. Appl. Mech. Eng.*, **298**, 407-427. <https://doi.org/10.1016/j.cma.2015.10.009>.
- Noorishad, J. and Tsang, C.F. (1996), "Coupled thermohydroelasticity phenomena in variably saturated fractured porous rocks-formulation and numerical solution", *Develop. Geotech. Eng.*, **79**, 93-134. [https://doi.org/10.1016/S0165-1250\(96\)80023-X](https://doi.org/10.1016/S0165-1250(96)80023-X).
- Ostermann, L. and Dinkler, D. (2014), "Modelling and numerical simulation of concrete structures subject to high temperatures", *Coupl. Syst. Mech.*, **3**(1), 73-88. <http://dx.doi.org/10.12989/csm.2014.3.1.053>.
- Terzaghi, K. (1944), *Theoretical Soil Mechanics*, Chapman and Hali, Limited John Wiler and Sons Inc., New York.
- Zienkiewicz, O.C. and Taylor, R.L. (2005), *The Finite Element Method, vols. I, II, III*, Elsevier.